MATERIALS SCIENCE

Dirac surface state–modulated spin dynamics in a ferrimagnetic insulator at room temperature

Chi Tang,[1]* Qi Song,[2,3]* Cui-Zu Chang,[4,5] Yadong Xu,[1] Yuichi Ohnuma,[6] Mamoru Matsuo,[6,7] Yawen Liu,[1] Wei Yuan,[2,3] Yunyan Yao,[2,3] Jagadeesh S. Moodera,[4,8,9] Sadamichi Maekawa,[5] Wei Han,[2,3] Jing Shi[1†]

This work demonstrates markedly modified spin dynamics of magnetic insulator (MI) by the spin momentum–locked Dirac surface states of the adjacent topological insulator (TI), which can be harnessed for spintronic applications. As the Bi concentration x is systematically tuned in 5-nm-thick $(Bi_xSb_{1-x})_2Te_3$ TI films, the weight of the surface relative to bulk states peaks at $x = 0.32$ when the chemical potential approaches the Dirac point. At this concentration, the Gilbert damping constant of the precessing magnetization in 10-nm-thick $Y_3Fe_5O_{12}$ MI films in the MI/TI heterostructures is enhanced by an order of magnitude, the largest among all concentrations. In addition, the MI acquires additional strong magnetic anisotropy that favors the in-plane orientation with similar Bi concentration dependence. These extraordinary effects of the Dirac surface states distinguish TI from other materials such as heavy metals in modulating spin dynamics of the neighboring magnetic layer.

INTRODUCTION

Topological insulators (TIs) are a new state of quantum matter with unique spin and charge properties owing to the nontrivial band topology and strong spin-orbit coupling (*1*). These properties can lead to a variety of exotic phenomena including topological magnetoelectric effects (*2*), quantum anomalous Hall effect (*3*), image magnetic monopoles (*4*), etc. A remarkable feature that profoundly affects spin and charge transport in TI is that electrons in Dirac surface states have their spin locked orthogonally to their momenta in two dimensions (*5*, *6*). Various spin and charge transport effects of such spin-momentum locking have been observed in spin valves with TI (*7*), spin Seebeck effect (*8*), inverse Edelstein effect (*9*–*13*), and spin-orbit torque switching (*14*, *15*). Strong coupling between electron spin and translational degrees of freedom can be exploited as an efficient way of manipulating spins and vice versa, which are essential for spintronics.

Devices revealing the aforementioned effects are often constructed in heterostructures containing TI and a ferromagnetic layer that serves as either a pure spin current source or a spin detector. Any spin-dependent effect on transport properties is conveniently measured through the metallic surface states. In the same heterostructures, the reverse effect, that is, the effect of the spin momentum–locked Dirac surface states on the spin dynamics of the magnetic layer, has not yet been systematically studied. It is known that a thin heavy metal such as Pt or W in contact with a magnetic material can cause broadening of the ferromagnetic resonance (FMR) linewidth, which is mainly attributed to the excess flow of spin current due to the spin pumping effect (*16*, *17*); however, the linewidth broadening is generally insignificant (~10 Oe) (*18*, *19*). In this regime, the effect is quantitatively described by the momentum sum of the imaginary part of the dynamical transverse spin susceptibility (*16*) or, alternatively, the spin-mixing conductance at the interface (*17*).

Here, we investigate the room temperature spin dynamics of yttrium iron garnet ($Y_3Fe_5O_{12}$ or YIG), a ferrimagnetic insulator, in heterostructures containing $(Bi_xSb_{1-x})_2Te_3$, a TI material. By systematically tuning the chemical potential of the TI with a fixed thickness, that is, five quintuple layers (QLs) or ~5 nm, via varying Bi concentration x, we control the weight of the surface states relative to the bulk states (*20*). An alternative way of controlling the surface state weight is to use electrostatic gating, which requires extensive materials work. In TI layers dominated by surface states, the direction of spins pumped into the Dirac surface states by FMR has to be locked in the plane. On the other hand, the spins in TI and those of YIG are exchange-coupled to each other at the interface. As a result, the direction of the precessing spins in YIG is forced to be aligned in the plane (Fig. 1A). Consequently, spin pumping into Dirac surface states is expected to give rise to strong damping of the precessing magnetization. We observe unprecedentedly large FMR linewidth broadening of YIG (up to 111 Oe at 9.6 GHz) when the chemical potential of the TI is tuned close to the Dirac point, which corresponds to a 15 times larger Gilbert damping constant. This marked enhancement in damping is accompanied by an anomalously large increase (~100%) in the easy-plane anisotropy of the YIG layer.

RESULTS

We choose YIG for the magnetic constituent in our heterostructures for several reasons to be described in Materials and Methods. Here, we have fabricated seven heterostructure samples with various Bi concentrations, x, ranging from 0 to 1. The $x = 0.32$ sample is the most insulating as indicated by the largest resistance at 300 K (Fig. 1B) and the largest negative slope in its temperature dependence (Fig. 1C), suggesting that the chemical potential is located close to the Dirac point. With x deviating from 0.32, the chemical potential is tuned away from the Dirac point (*20*). In Bi_2Te_3 ($x = 1$) and Sb_2Te_3 ($x = 0$), the chemical potential is located in the bulk conduction and valence bands, respectively.

We measure FMR spectra with both cavity and broadbrand coplanar waveguide FMR setups. Before TI layer deposition, cavity FMR measurements are performed on all 10-nm-thick YIG films at

[1]Department of Physics and Astronomy, University of California, Riverside, Riverside, CA 92521, USA. [2]International Center for Quantum Materials, School of Physics, Peking University, Beijing 100871, China. [3]Collaborative Innovation Center of Quantum Matter, Beijing 100871, China. [4]Francis Bitter Magnet Laboratory, Massachusetts Institute of Technology, Cambridge, MA 02139, USA. [5]Department of Physics, The Pennsylvania State University, University Park, PA 16802, USA. [6]Advanced Science Research Center, Japan Atomic Energy Agency, Tokai 319-1195, Ibaraki, Japan. [7]Advanced Institute for Materials Research, Tohoku University, Sendai 980-8577, Miyagi, Japan. [8]Department of Physics, Massachusetts Institute of Technology, Cambridge, MA 02139, USA. [9]Plasma Science and Fusion Center, Massachusetts Institute of Technology, Cambridge, MA 02139, USA.
*These authors contributed equally to this work.
†Corresponding author. Email: jing.shi@ucr.edu

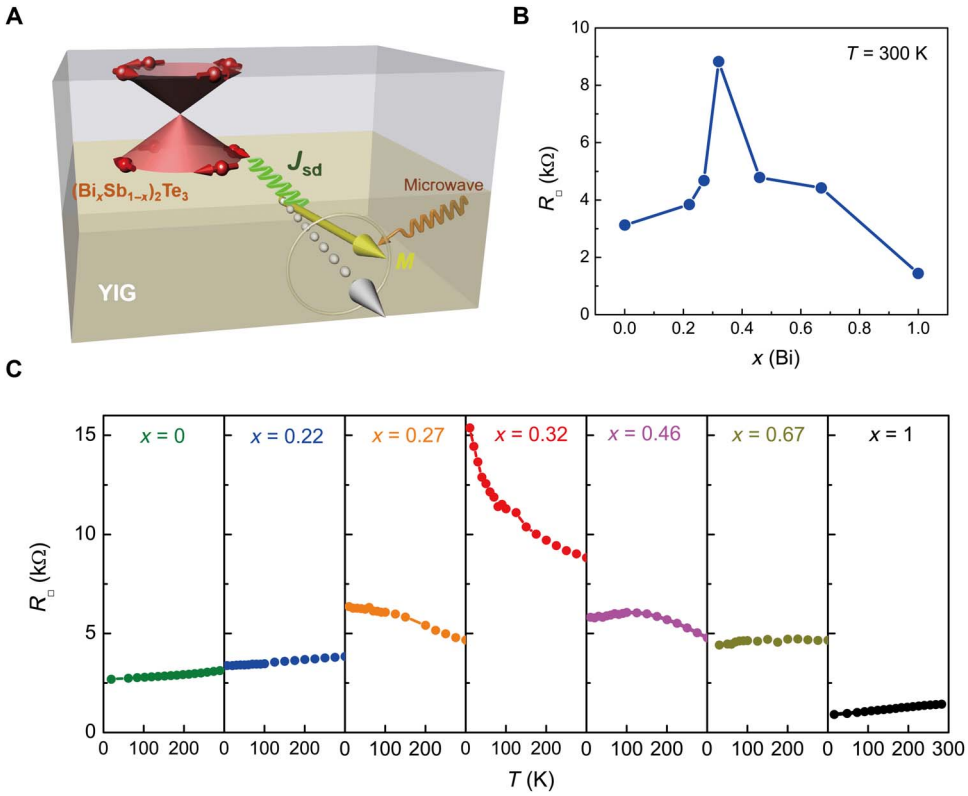

Fig. 1. FMR measurement principle and TI properties. (**A**) Schematic drawing of magnetization dynamics in YIG interfaced with TI in which the spin of the surface state electron is locked to momentum. (**B**) Room temperature sheet resistance of $(Bi_xSb_{1-x})_2Te_3$ with different Bi concentrations. (**C**) Temperature dependence of the sheet resistance of seven YIG (10 nm)/$(Bi_xSb_{1-x})_2Te_3$ (five QLs) heterostructures.

room temperature using a Bruker 9.6 GHz X-band EMX EPR spectrometer. Figure 2B (red curve) shows an FMR derivative absorption spectrum of a representative YIG film with an in-plane magnetic field, which can be well fitted with a single Lorentzian derivative. The peak-to-peak linewidth ΔH_{pp} of 7.0 Oe and resonance field H_{res} of 2434.0 Oe are obtained from the fitting. Such a narrow linewidth indicates high YIG film quality. The mean values of both ΔH_{pp} and H_{res} for all seven samples are 10.2 ± 3.1 Oe and 2394.5 ± 40.2 Oe, respectively. When FMR is performed as a function of the polar angles θ_H (defined in Fig. 2A), the θ_H dependence of both quantities shows very small variations for all seven YIG samples (fig. S2), indicating a tight control over the YIG film quality.

To study the effect of the TI Dirac surface states on YIG spin dynamics, we compare the YIG FMR spectra taken before and after the TI growth. Figure 2B shows a direct comparison between the two representative FMR spectra taken with in-plane fields before and after the growth of a five-QL Sb_2Te_3 ($x = 0$) film. Two distinct differences stand out. First, H_{res} is shifted to a lower field by 207 Oe, that is, from 2434 to 2227 Oe, indicating a large effect on magnetic anisotropy upon adding the five-QL Sb_2Te_3. Second, the FMR linewidth ΔH_{pp} is broadened by seven times. To more accurately determine the effective anisotropy field change, we measure FMR of both YIG/Sb_2Te_3 and a YIG reference sample as a function of polar angle θ_H (*21*, *22*). Figure 2C shows the spectra at selected polar angles between the in-plane (θ_H = 90°) and out-of-plane (θ_H = 0°) magnetic field orientations. The YIG reference sample has relatively narrow FMR linewidth for all polar angles. In the meantime, H_{res} decreases monotonically from ~5560 Oe for H out-of-plane to ~2434 Oe for H in-plane, consistent

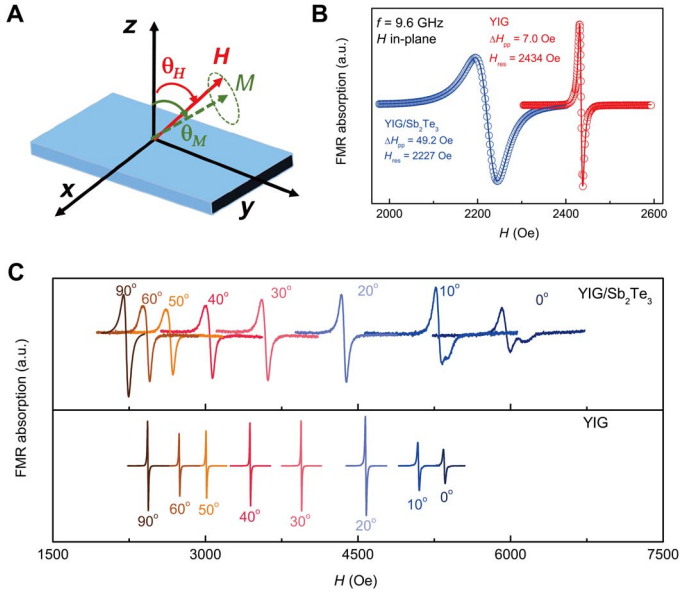

Fig. 2. YIG FMR spectra with and without TI. (**A**) Definition of polar angles θ_H and θ_M in FMR measurements. (**B**) FMR derivative absorption spectra of YIG/Sb_2Te_3 and YIG reference sample at a frequency of 9.6 GHz with magnetic field applied in-plane (θ_H = 90°). The solid lines are the best fits to extract the resonance field H_{res} and peak-to-peak linewidth ΔH_{pp}. a.u., arbitrary units. (**C**) FMR derivative absorption spectra of YIG/Sb_2Te_3 and YIG reference sample with the polar angle θ_H ranging from 0° (out-of-plane) to 90° (in-plane) at 300 K. The extra peak-like feature on the high-field side of the resonance at 0° and 10° is also observed in some other samples, which could be caused by minor inhomogeneity change in YIG due to the presence of the TI layer.

with the behavior of nanometer-thick YIG films with easy-plane magnetic anisotropy (*23*). With five-QL Sb_2Te_3 on top, however, marked differences can be readily identified as shown in Fig. 2C (top panel): significant broadening of ΔH_{pp} and large shift in H_{res}. H_{res} shift occurs at all angles; hence, the overall H_{res} range is greatly expanded, that is, between 2227 and 6000 Oe. These marked effects are not seen in heterostructures containing thin heavy metal layers such as Pt (*18*).

The differences in both ΔH_{pp} and H_{res} caused by the five-QL Sb_2Te_3 suggest their origin in the band structure of TI. To study the effects of the TI Dirac surface states, we compare the FMR results in all seven samples in which the surface-to-bulk ratio systematically varies. We first study the effect of varying x on the easy-plane magnetic anisotropy. We plot H_{res} as a function of θ_H in Fig. 3A for all seven YIG/$(Bi_xSb_{1-x})_2Te_3$ samples plus a YIG reference film. The angular dependence data can be fitted reasonably well with the shape anisotropy plus a uniaxial anisotropy term, both in the form of $\cos^2\theta$. As is routinely done in literature (*21*), we solve three transcendental equations numerically and seek the least-square fitting results. Note that, if the uniaxial anisotropy term is negative, then it simply represents easy-plane anisotropy. We find that it is indeed negative, that is, there is additional easy-plane anisotropy in all seven samples. By fitting the polar angle dependence, we obtain the two best-fit parameters, $4\pi M_{eff}$ and the g-factor, for each sample. The effective anisotropy field is defined as $4\pi M_{eff} = 4\pi M_s + H_{an}$, where $4\pi M_s$ and H_{an} denote the demagnetizing field and an effective easy-plane (positive) magnetic anisotropy field, respectively (*24*). The best-fit parameters are summarized in table S1. The extracted $4\pi M_{eff}$ is plotted in Fig. 3B. Because the demagnetizing field $4\pi M_s$ is about 1780 Oe, $4\pi M_{eff}$ is clearly larger than $4\pi M_s$ in all samples. Furthermore, $4\pi M_{eff}$ depends on x. For the two most metallic TI films, that is, $x = 0$ and $x = 1$, $4\pi M_{eff}$ is increased by 420 and 460 Oe, which accounts for 23% and 26% of its demagnetizing field $4\pi M_s$, respectively. In comparison, the corresponding increase is only 5% in YIG/Pt (fig. S3A). As the chemical potential is tuned into the bandgap, that is, surface states becoming dominant, $4\pi M_{eff}$ increases further and peaks in the most insulating sample ($x = 0.32$), reaching 3800 Oe. This increase represents nearly a 100% enhancement over the YIG demagnetizing field $4\pi M_s$.

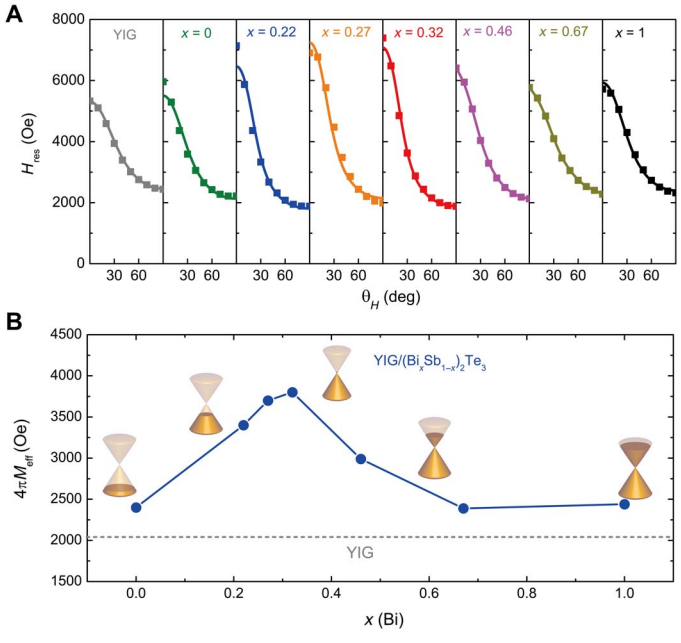

Fig. 3. Extracted $4\pi M_{eff}$ from FMR polar angle dependence fitting. (**A**) Polar angle θ_H dependence of FMR resonance field H_{res} for all seven YIG (10 nm)/$(Bi_xSb_{1-x})_2Te_3$ (five QLs) samples and YIG reference sample. Solid curves are the best fits. (**B**) Bi concentration dependence of extracted effective anisotropy field $4\pi M_{eff}$ obtained from fitting in (A) for all seven YIG (10 nm)/$(Bi_xSb_{1-x})_2Te_3$ (five QLs) samples. The gray dashed line is the $4\pi M_{eff}$ value for the YIG reference sample.

A common origin of enhanced magnetic anisotropy in thin films is related to the interface strain. In $(Bi_xSb_{1-x})_2Te_3$, the interaction between the neighboring Te-Bi/Sb-Te-Bi/Sb-Te QLs is of the van der Waals type. Between yttrium iron garnet and TI, there is no epitaxial relation because of widely different lattice structures; therefore, the strain and strain-induced anisotropy are expected to be small at the YIG-TI interface for all samples. Another possibility of the enhanced $4\pi M_{eff}$ is an increased demagnetizing field. If part of TI becomes ferromagnetic, then it can, in principle, cause an increase in $4\pi M_s$. We exclude this possibility with the following arguments. First, such a proximity-induced moment, if exists, can only come from a few atomic layers at the interface and is clearly too small to account for the observed 100% increase. Our magnetization measurements do not support this possibility either (fig. S5). The same magnetometry results do not show any clear Bi concentration dependence within experimental uncertainty. The proximity effect in YIG/TI heterostructures occurs at much lower temperatures (<150 K) as reported in previous studies (*8*, *25*). In addition, the T_c of the induced ferromagnetism in TI was found to be uncorrected with the chemical potential position of the TI (*25*). In our data, the $4\pi M_{eff}$ enhancement follows the same trend as the resistivity, as shown in Fig. 1C. From these analyses, we conclude that the enhanced effective anisotropy originates from the Dirac surface states.

The cavity FMR measurements have already indicated anomalously broadened FMR linewidth at a particular microwave frequency. To extract the Gilbert damping constant α, we perform broadband FMR measurements using a coplanar waveguide setup for all YIG/TI samples up to 12 GHz. Representative transmission data S_{21} in Fig. 4A show the FMR absorption of YIG/Sb_2Te_3 with several frequencies. Both FMR resonance field shift and linewidth broadening display the same trend in Fig. 4B. The half width at half maximum, $\Delta H = \sqrt{3}\Delta H_{pp}/2$, is extracted by fitting a Lorentzian function to each S_{21} spectrum up to 12 GHz and then plotted in Fig. 4C for all samples. A linear relation between ΔH and frequency is observed, and α can be calculated by (*24*)

$$\Delta H = \frac{2\pi}{\gamma}\alpha f + \Delta H_0 \quad (1)$$

where γ and ΔH_0 are the gyromagnetic ratio and the inhomogeneity linewidth broadening, respectively. Figure 4D shows α versus x for all samples. α peaks at $x = 0.32$ as well, that is, in the most insulating sample, similar to the resistivity and the effective anisotropy field. Compared to the two most metallic samples with $\alpha = 8.0 \times 10^{-3}$ for $x = 0$ (or Sb_2Te_3) and $\alpha = 4.5 \times 10^{-3}$ for $x = 1$ (or Bi_2Te_3), α reaches the maximum value of 2.2×10^{-2} for $x = 0.32$, which is an order of magnitude larger than that of the bare YIG films (average value of 1.5×10^{-3}). In comparison, α in YIG/Pt is only twice as large as that in the YIG reference, as shown in fig. S4B. In addition, α shows the same trend as that of the resistivity and effective anisotropy. These facts suggest a common origin, of the observed modulated spin dynamics that is, the special band structures of the TI surface states rather than the spin-orbit coupling of the constituent elements. The latter effect would imply a monotonically increasing trend as more Bi atoms are incorporated.

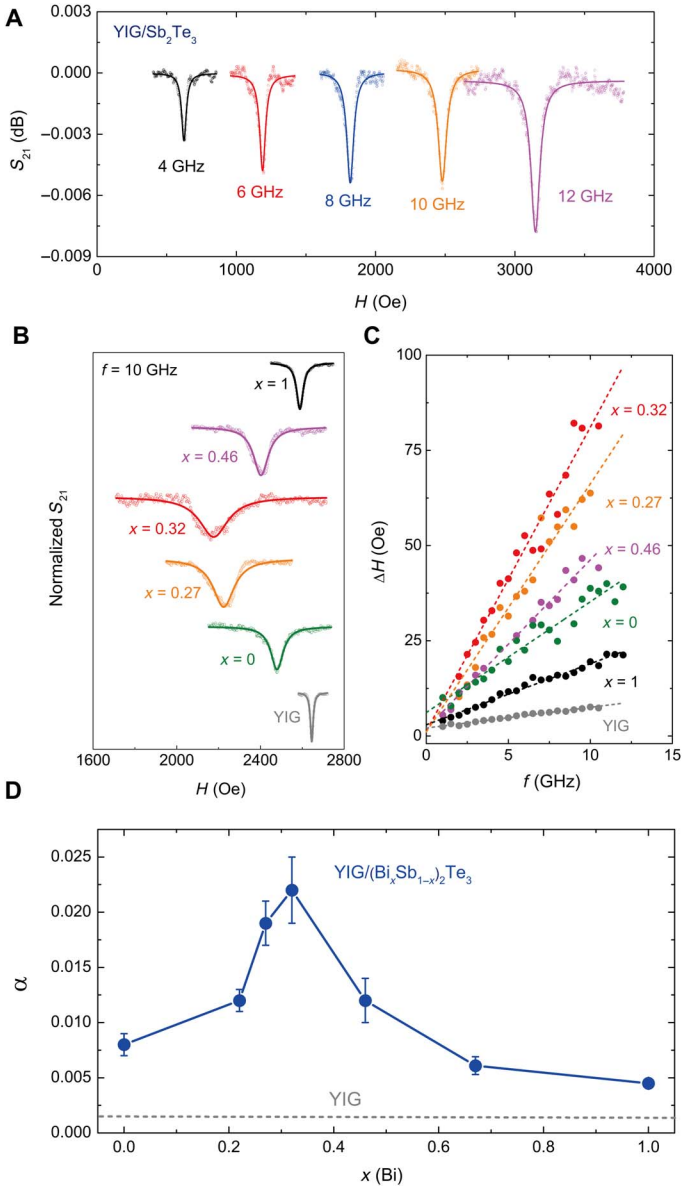

Fig. 4. Extracted Gilbert damping from FMR linewidth fitting. (**A**) FMR transmission spectra $_{S_{21}}$ for YIG/Sb_2Te_3 for different chosen frequencies: 4, 6, 8, 10, and 12 GHz at 300 K after background subtraction. (**B**) Normalized FMR spectra $_{S_{21}}$ at a fixed frequency of 10 GHz with an applied in-plane static field for YIG/$(Bi_xSb_{1-x})_2Te_3$ samples with different Bi concentrations and YIG reference sample. (**C**) Frequency dependence of FMR linewidth for all seven YIG/TI samples and YIG reference sample. The resonance peak height is reduced in samples with increased damping constant, which causes poor Lorentzian fitting and, consequently, large apparent noise in extracted linewidth. (**D**) Bi concentration (x) dependence of the Gilbert damping constant α extracted from the slope of the straight lines in (C).

DISCUSSION

We now show that these three effects are actually connected and given by the spin-momentum locking properties of the TI Dirac surface states. The spins ($\vec{\sigma}$) of TI and the spins ($\vec{S}$) of YIG are coupled by the exchange interaction expressed as (*26*, *27*) $H = J_{sd}\vec{\sigma}\cdot\vec{S}$, with J_{sd} being the exchange constant at the interface. We note that the spins in TI lie in the plane because of the spin-momentum locking. Therefore, the spins in YIG are pulled toward the plane as well. This pulling effect induces the easy-plane anisotropy given by

$$E_{an} = -\frac{1}{2}(\chi_{//} - \chi_{\perp})M^2 \quad (2)$$

where $\chi_{//}$ and $\chi_{\perp}$ are the in-plane and out-of-plane components of the spin susceptibility in TI, respectively, and M is the magnetization of YIG. In particular, when the chemical potential is close to the Dirac point, $\chi_{\perp}$ is strongly suppressed because of the gap (*28*), and thus, $\chi_{//} \gg \chi_{\perp}$. The spin susceptibility of the TI gives rise to the easy-plane magnetic anisotropy field by $H_{an} = -\frac{\partial E_{an}}{\partial M}$.

The same interfacial exchange interaction also affects spin pumping (*16*); the spin precession of YIG in FMR results in the motion of spins in TI. The induced spin current (I_s) in TI is expressed as

$$I_s \propto J_{sd}^2 I_m \chi^{+-}(\omega) \quad (3)$$

where $\chi^{+-}(\omega)$ is the transverse component in TI to the magnetization direction of YIG, and ω is the FMR frequency. We note that, because the spin Seebeck effect is due to the spin pumping by heat (*26*, *27*), it is also given by $\chi^{+-}(\omega)$ but integrated over ω in the range of the thermal distribution of spin fluctuations. The susceptibility is calculated by taking into account the direct transition near the Fermi level because of the spin-momentum locking in TI (see the Supplementary Materials for details). Because the resonance frequency (a few gigahertz) is much smaller than the energy gap of TI (~0.3 eV) (*29*), the direct transition is more effective when the Fermi energy is near the Dirac point. As a result, the spin pumping (the Gilbert damping) is significantly enhanced near the Dirac point. This model also explains enhanced spin Seebeck effect reported previously (*8*).

In summary, we have observed marked modifications of YIG spin dynamics by spin momentum–locked surfaces of a thin TI layer in high-quality YIG/TI heterostructures with different Bi/Sb ratios. The spin-momentum locking in TI provides not only a sensitive detection of the magnetic state in magnetic materials serving as a spin current source but also an active way of manipulating ultrafast magnetization dynamics and magnetic anisotropy with the unique properties of the topological Dirac surface states, which offers exciting opportunities for potential spintronic applications.

MATERIALS AND METHODS

Choice of YIG

We chose 10-nm-thick YIG films as the magnetic insulator (MI) layers in all MI/TI heterostructures. First, YIG in general has a very small Gilbert damping constant α (~3×10^{-5} in crystals and ~10^{-3} in 10-nm-thick YIG films), and the FMR linewidth is relatively narrow (~10 Oe at ~10 GHz for thin films). Therefore, small linewidth changes can be easily detected. Second, YIG films are prepared first with high temperatures (~800°C) with pulsed laser deposition and rapid thermal annealing, and the TI layers are grown at much lower temperatures (~230°C) after with molecular beam epitaxy (MBE). This growth sequence and the large temperature difference prevents serious intermixing across the interface. In our heterostructures, YIG is atomically flat, which ensures the flat YIG-TI interface. Third, similar to our previous spin Seebeck effect study (*8*), here, we conducted FMR measurements at room temperature that was well above that of the induced

ferromagnetism in the TI surface layer. Consequently, the dynamic behavior of YIG was not affected by the induced ferromagnetism in TI (*18*).

Heterostructure growth

Thin YIG films were grown on epi-ready lattice-matched single crystal GGG (111) substrates via pulsed laser deposition. The detailed growth recipe of YIG films was described in a previous paper (*30*). To fabricate high-quality YIG/$(Bi_xSb_{1-x})_2Te_3$ heterostructures with various Bi concentrations (x = 0, 0.22, 0.27, 0.32, 0.46, 0.67, and 1 in this study), we then transferred YIG (111) films to an ultrahigh vacuum MBE system with the base pressure better than 5×10^{-10} Torr for TI growth. High-purity Bi (99.999%), Sb (99.9999%), and Te (99.9999%) were evaporated from Knudsen effusion cells. During the growth, the YIG substrate was kept at 230°C, and the growth rate of TI was ~0.2 QL/min. The heterostructure film was covered with a 5-nm Te protection layer before taken out of the MBE chamber for the FMR measurements.

FMR measurements

The polar angle–dependent FMR measurements for all samples were performed using a Bruker 9.6-GHz X-band EMX EPR spectrometer. Samples could be rotated with respect to the static field direction from the in-plane to out-of-plane geometry, with a protractor reading the angle precisely.

The Gilbert damping constant measurements were conducted by a broadband FMR using a coplanar waveguide setup. The forward amplitude of complex transmission coefficients (S_{21}) was recorded by the vector network analyzer (E5071C, Agilent Technologies) connected to a straight-line coplanar waveguide (*31*). Each sample was attached to the waveguide, and the measurement was performed, with the frequency sweeping from 1 to 12 GHz at a fixed magnetic field, which could be varied up to 4000 Oe.

SUPPLEMENTARY MATERIALS

Supplementary material for this article is available at http://advances.sciencemag.org/cgi/content/full/4/6/eaas8660/DC1

fig. S1. Crystal structure and surface morphology.
fig. S2. FMR resonance field and linewidth for all YIG films.
fig. S3. Effect of Pt on YIG resonance characteristics.
fig. S4. Comparison of FMR between YIG/TI and YIG/Pt.
fig. S5. Comparison of total effective anisotropy field and demagnetizing field.
fig. S6. High-resolution transmission electron microscope image of a representative YIG/TI sample.
fig. S7. TI surface state dispersion.
fig. S8. Direct transition of TI conduction electrons driven by spin pumping.
table S1. Two parameters (that is, $4\pi M_{eff}$ and $\gamma/2\pi$) obtained from fitting.
References (*32*, *33*)

REFERENCES AND NOTES

1. X.-L. Qi, S.-C. Zhang, Topological insulators and superconductors. *Rev. Mod. Phys.* **83**, 1057–1110 (2011).
2. X.-L. Qi, T. L. Hughes, S.-C. Zhang, Topological field theory of time-reversal invariant insulators. *Phys. Rev. B* **78**, 195424 (2008).
3. C.-Z. Chang, J. Zhang, X. Feng, J. Shen, Z. Zhang, M. Guo, K. Li, Y. Ou, P. Wei, L.-L. Wang, Z.-Q. Ji, Y. Feng, S. Ji, X. Chen, J. Jia, X. Dai, Z. Fang, S.-C. Zhang, K. He, Y. Wang, L. Lu, X.-C. Ma, Q.-K. Xue, Experimental observation of the quantum anomalous Hall effect in a magnetic topological insulator. *Science* **340**, 167–170 (2013).
4. X.-L. Qi, R. Li, J. Zang, S.-C. Zhang, Inducing a magnetic monopole with topological surface states. *Science* **323**, 1184–1187 (2009).
5. D. Hsieh, Y. Xia, D. Qian, L. Wray, J. H. Dil, F. Meier, J. Osterwalder, L. Patthey, J. G. Checkelsky, N. P. Ong, A. V. Fedorov, H. Lin, A. Bansil, D. Grauer, Y. S. Hor, R. J. Cava, M. Z. Hasan, A tunable topological insulator in the spin helical Dirac transport regime. *Nature* **460**, 1101–1105 (2009).
6. Z.-H. Pan, E. Vescovo, A. V. Fedorov, D. Gardner, Y. S. Lee, S. Chu, G. D. Gu, T. Valla, Electronic structure of the topological insulator Bi_2Se_3 using angle-resolved photoemission spectroscopy: Evidence for a nearly full surface spin polarization. *Phys. Rev. Lett.* **106**, 257004 (2011).
7. C. H. Li, O. M. J. van't Erve, J. T. Robinson, Y. Liu, L. Li, B. T. Jonker, Electrical detection of charge-current-induced spin polarization due to spin-momentum locking in Bi_2Se_3. *Nat. Nanotechnol.* **9**, 218–224 (2014).
8. Z. Jiang, C.-Z. Chang, M. R. Masir, C. Tang, Y. Xu, J. S. Moodera, A. H. MacDonald, J. Shi, Enhanced spin Seebeck effect signal due to spin-momentum locked topological surface states. *Nat. Commun.* **7**, 11458 (2016).
9. Y. Shiomi, K. Nomura, Y. Kajiwara, K. Eto, M. Novak, K. Segawa, Y. Ando, E. Saitoh, Spin-electricity conversion induced by spin injection into topological insulators. *Phys. Rev. Lett.* **113**, 196601 (2014).
10. M. Jamali, J. S. Lee, J. S. Jeong, F. Mahfouzi, Y. Lv, Z. Zhao, B. K. Nikolić, K. A. Mkhoyan, N. Samarth, J.-P. Wang, Giant spin pumping and inverse spin Hall effect in the presence of surface and bulk spin-orbit coupling of topological insulator Bi_2Se_3. *Nano Lett.* **15**, 7126–7132 (2015).
11. H. Wang, J. Kally, J. S. Lee, T. Liu, H. Chang, D. R. Hickey, K. A. Mkhoyan, M. Wu, A. Richardella, N. Samarth, Surface-state-dominated spin-charge current conversion in topological-insulator–ferromagnetic-insulator heterostructures. *Phys. Rev. Lett.* **117**, 076601 (2016).
12. K. Kondou, R. Yoshimi, A. Tsukazaki, Y. Fukuma, J. Matsuno, K. S. Takahashi, M. Kawasaki, Y. Tokura, Y. Otani, Fermi-level-dependent charge-to-spin current conversion by Dirac surface states of topological insulators. *Nat. Phys.* **12**, 1027–1031 (2016).
13. Q. Song, J. Mi, D. Zhao, T. Su, W. Yuan, W. Xing, Y. Chen, T. Wang, T. Wu, X. H. Chen, X. C. Xie, C. Zhang, J. Shi, W. Han, Spin injection and inverse Edelstein effect in the surface states of topological Kondo insulator SmB_6. *Nat. Commun.* **7**, 13485 (2016).
14. Y. Fan, P. Upadhyaya, X. Kou, M. Lang, S. Takei, Z. Wang, J. Tang, L. He, L.-T. Chang, M. Montazeri, G. Yu, W. Jiang, T. Nie, R. N. Schwartz, Y. Tserkovnyak, K. L. Wang, Magnetization switching through giant spin-orbit torque in a magnetically doped topological insulator heterostructure. *Nat. Mater.* **13**, 699–704 (2014).
15. Y. Fan, X. Kou, P. Upadhyaya, Q. Shao, L. Pan, M. Lang, X. Che, J. Tang, M. Montazeri, K. Murata, L.-T. Chang, M. Akyol, G. Yu, T. Nie, K. L. Wong, J. Liu, Y. Wang, Y. Tserkovnyak, K. L. Wang, Electric-field control of spin-orbit torque in a magnetically doped topological insulator. *Nat. Nanotechnol.* **11**, 352–359 (2016).
16. Y. Ohnuma, H. Adachi, E. Saitoh, S. Maekawa, Enhanced dc spin pumping into a fluctuating ferromagnet near T_C. *Phys. Rev. B* **89**, 174417 (2014).
17. Y. Tserkovnyak, A. Brataas, G. E. W. Bauer, Spin pumping and magnetization dynamics in metallic multilayers. *Phys. Rev. B* **66**, 224403 (2002).
18. Y. Sun, H. Chang, M. Kabatek, Y.-Y. Song, Z. Wang, M. Jantz, W. Schneider, M. Wu, E. Montoya, B. Kardasz, B. Heinrich, S. G. E. te Velthuis, H. Schultheiss, A. Hoffmann, Damping in yttrium iron garnet nanoscale films capped by platinum. *Phys. Rev. Lett.* **111**, 106601 (2013).
19. C. Du, H. Wang, F. Yang, P. C. Hammel, Enhancement of pure spin currents in spin pumping $Y_3Fe_5O_{12}$/Cu/Metal trilayers through spin conductance matching. *Phys. Rev. Appl.* **1**, 044004 (2014).
20. J. Zhang, C.-Z. Chang, Z. Zhang, J. Wen, X. Feng, K. Li, M. Liu, K. He, L. Wang, X. Chen, Q.-K. Xue, X. Ma, Y. Wang, Band structure engineering in $(Bi_{1-x}Sb_x)_2Te_3$ ternary topological insulators. *Nat. Commun.* **2**, 574 (2011).
21. S. Mizukami, Y. Ando, T. Miyazaki, The study on ferromagnetic resonance linewidth for NM/80NiFe/NM (NM = Cu, Ta, Pd and Pt) Films. *Jpn. J. Appl. Phys.* **40**, 580–585 (2001).
22. X. Liu, W. L. Lim, L. V. Titova, M. Dobrowolska, J. K. Furdyna, Perpendicular magnetization reversal, magnetic anisotropy, multistep spin switching, and domain nucleation and expansion in $Ga_{1-x}Mn_xAs$ films. *J. Appl. Phys.* **98**, 063904 (2005).
23. C. Tang, P. Sellappan, Y. Liu, Y. Xu, J. E. Garay, J. Shi, Anomalous Hall hysteresis in $Tm_3Fe_5O_{12}$/Pt with strain-induced perpendicular magnetic anisotropy. *Phys. Rev. B* **94**, 140403(R) (2016).
24. S. V. Vonsovskiĭ, *Ferromagnetic Resonance* (Pergamon, 1966).
25. Z. Jiang, C.-Z. Chang, C. Tang, P. Wei, J. S. Moodera, J. Shi, Independent tuning of electronic properties and induced ferromagnetism in topological insulators with heterostructure approach. *Nano Lett.* **15**, 5835–5840 (2015).
26. H. Adachi, J.-i. Ohe, S. Takahashi, S. Maekawa, Linear-response theory of spin Seebeck effect in ferromagnetic insulators. *Phys. Rev. B* **83**, 094410 (2011).
27. H. Adachi, K.-i. Uchida, E. Saitoh, S. Maekawa, Theory of the spin Seebeck effect. *Rep. Prog. Phys.* **76**, 036501 (2013).
28. M. M. Vazifeh, M. Franz, Spin response of electrons on the surface of a topological insulator. *Phys. Rev. B* **86**, 045401 (2012).
29. Y. L. Chen, J. G. Analytis, J.-H. Chu, Z. K. Liu, S.-K. Mo, X. L. Qi, H. J. Zhang, D. H. Lu, X. Dai, Z. Fang, S. C. Zhang, I. R. Fisher, Z. Hussain, Z.-X. Shen, Experimental realization of a three-dimensional topological insulator, Bi_2Te_3. *Science* **325**, 178–181 (2009).

30. C. Tang, M. Aldosary, Z. Jiang, H. Chang, B. Madon, K. Chan, M. Wu, J. E. Garay, J. Shi, Exquisite growth control and magnetic properties of yttrium iron garnet thin films. *Appl. Phys. Lett.* **108**, 102403 (2016).
31. Y. Zhao, Q. Song, S.-H. Yang, T. Su, W. Yuan, S. S. P. Parkin, J. Shi, W. Han, Experimental investigation of temperature-dependent Gilbert damping in permalloy thin films. *Sci. Rep.* **6**, 22890 (2016).
32. Y. Ohnuma, H. Adachi, E. Saitoh, S. Maekawa, Magnon instability driven by heat current in magnetic bilayers. *Phys. Rev. B* **92**, 224404 (2015).
33. S. Maekawa, H. Adachi, K.-i. Uchida, J. Ieda, E. Saitoh, Spin current: Experimental and theoretical aspects. *J. Phys. Soc. Jpn.* **82**, 102002 (2013).

Acknowledgments: We acknowledge the assistance from N. Samarth and J. Kally for the sample preparation and useful discussions with Z. Shi, J. Li, V. Ortiz, and M. Aldosary. **Funding:** This work was supported as part of the Spins and Heat in Nanoscale Electronic Systems, an Energy Frontier Research Center funded by the U.S. Department of Energy, Office of Science, Basic Energy Sciences under award no. SC0012670 (C.T., Y.X., Y.L., and J.S.). Q.S., W.Y., Y.Y., and W.H. acknowledge the support of the National Basic Research Programs of China (973 grants 2014CB920902 and 2015CB921104) and the National Natural Science Foundation of China (grant 11574006). C.-Z.C. and J.S.M. acknowledge the support of the NSF under grant nos. DMR-1207469 and 1700137, the Office of Naval Research under grant nos. N00014-13-1- 0301 and N00014-16-1-2657, and the STC (Science and Technology Center) Center for Integrated Quantum Materials under NSF grant no. DMR-1231319. Y.O., M.M., and S.M. acknowledge the support of the Exploratory Research for Advanced Technology–Japan Science and Technology Agency (JPMJER1402) and the Grant-in-Aid for Scientific Research on Innovative Areas Nano Spin Conversion Science (26103006), Grant-in-Aid for Scientific Research C (JP15K05153), and Grant-in-Aid for Scientific Research B (JP16H04023 and JP17H02927) from the Ministry of Education, Culture, Sports, Science and Technology, Japan. **Author contributions:** J.S. conceived and supervised the experiments. C.T. grew the YIG MI thin films and performed the cavity FMR measurements and data analysis with the help of Y.L. Q.S. performed the broadband FMR measurements and data analysis with the help of W.Y. and Y.Y. and the supervision of W.H. Y.X. performed the transmission electron microscopy sample preparation. C.-Z.C. grew the TI thin films on YIG to form heterostructures with the supervision of J.S.M. Y.O., M.M., and S.M. did the theoretical calculations. All authors participated in the preparation of the final manuscript. **Competing interests:** The authors declare that they have no competing interests. **Data and materials availability:** All data needed to evaluate the conclusions in the paper are present in the paper and/or the Supplementary Materials. Additional data related to this paper may be requested from the authors.

Submitted 27 December 2017
Accepted 20 April 2018
Published 1 June 2018
10.1126/sciadv.aas8660

Citation: C. Tang, Q. Song, C.-Z. Chang, Y. Xu, Y. Ohnuma, M. Matsuo, Y. Liu, W. Yuan, Y. Yao, J. S. Moodera, S. Maekawa, W. Han, J. Shi, Dirac surface state–modulated spin dynamics in a ferrimagnetic insulator at room temperature. *Sci. Adv.* **4**, eaas8660 (2018).